A Model Investigation of Aerosol-Induced Changes in Boreal Winter Extratropical Circulation

Y. MING AND V. RAMASWAMY

NOAA/Geophysical Fluid Dynamics Laboratory, Princeton, New Jersey

GANG CHEN

Department of Earth and Atmospheric Sciences, Cornell University, Ithaca, New York

ABSTRACT

The authors examine the key characteristics of the boreal winter extratropical circulation changes in response to anthropogenic aerosols, simulated with a coupled atmosphere–slab ocean general circulation model. The zonal-mean response features a pronounced equatorward shift of the Northern Hemisphere subtropical jet owing to the midlatitude aerosol cooling. The circulation changes also show strong zonal asymmetry. In particular, the cooling is more concentrated over the North Pacific than over the North Atlantic despite similar regional forcings. With the help of an idealized model, the authors demonstrate that the zonally asymmetrical response is linked tightly to the stationary Rossby waves excited by the anomalous diabatic heating over the tropical east Pacific. The altered wave pattern leads to a southeastward shift of the Aleutian low (and associated changes in winds and precipitation), while leaving the North Atlantic circulation relatively unchanged.

Despite the rich circulation changes, the variations in the extratropical meridional latent heat transport are controlled strongly by the dependence of atmospheric moisture content on temperature. This suggests that one can project reliably the changes in extratropical zonal-mean precipitation solely from the global-mean temperature change, even without a good knowledge of the detailed circulation changes caused by aerosols. On the other hand, such knowledge is indispensable for understanding zonally asymmetrical (regional) precipitation changes.

1. Introduction

The Earth's climate system comprises distinct regimes, depending mainly on latitude and season. When one moves from the tropics into the wintertime extratropics, stationary Rossby waves and baroclinic eddies overtake the time-mean flow as the main mechanism of poleward energy and moisture transport. In light of the fundamental differences between the two climate regimes, we use this paper to examine specifically the impacts of aerosols on the boreal winter extratropical circulation. The other two papers in the present series focus mainly on the tropical and monsoon circulations, respectively (Ming and Ramaswamy 2011; Y. Ming et al. 2011, unpublished manuscript).

The general circulation model (GCM)-simulated climate response to global warming has been studied extensively (e.g., Hall et al. 1994; Kushner et al. 2001; Yin 2005; Lu et al. 2007; Lorenz and DeWeaver 2007). More specifically, Hall et al. (1994) and Yin (2005) examined the changes in the characteristics of storm tracks, while Lu et al. (2007) focused on the Hadley circulation. Kushner et al. (2001) studied how the warming may affect the Southern Hemisphere (SH) extratropical circulation and the southern annular mode. Lorenz and DeWeaver (2007) used a simple dry GCM to explore the influence of an increase in tropopause height on the midlatitude circulation. A much discussed phenomenon was the poleward displacement of the subtropical jet streams and storm tracks, accompanied by an expansion of the Hadley circulation. This has been linked to increased subtropical static stability (e.g., Frierson et al. 2007; Lu et al. 2008), to stronger meridional temperature gradients near the tropopause as a result of concurrent

Corresponding author address: Yi Ming, NOAA/Geophysical Fluid Dynamics Laboratory, P. O. Box 308, Princeton, NJ 08542.
E-mail: yi.ming@noaa.gov

tropical upper-tropospheric warming and stratospheric cooling (e.g., Chen and Held 2007; Chen et al. 2008), and to a higher tropopause (Lorenz and DeWeaver 2007). A few studies (e.g., Krisjánsson et al. 2005; Ming and Ramaswamy 2009) identified an equatorward shift of storm tracks as part of the response to aerosol cooling. This result is in qualitative agreement with the past work on a similar shift in the cold climate during the last glacial maximum (LGM; Williams and Bryan 2006; Toggweiler et al. 2006). One may be tempted to draw the conclusion that both the warming and cooling cases are governed by the same mechanism, and the direction of the shift depends only on the sign of temperature change. Consistent with this line of thinking, Fischer-Bruns et al. (2009) argued that aerosol cooling merely offsets the warming-induced poleward shift by lessening the decrease in baroclinicity. In this paper, we try to shed more light on this specific issue.

It is useful to think of aerosol impacts on the extratropics in terms of physical mechanisms. Aerosols are abundant in the Northern Hemisphere (NH) mid-latitudes, where the major industrial regions lie. By scattering and/or absorbing insolation (either directly or through altering clouds), they pose *direct* thermal forcing on circulation. Ming and Ramaswamy (2011) and Y. Ming et al. (2011, unpublished manuscript) showed the richness of the tropical response to aerosols. It is well known that a change in the tropical state can influence the extratropical climate. There is a large body of work that documented the crucial role of stationary Rossby waves in establishing the teleconnection between the tropics and extratropics (e.g., Lau 1997; Alexander et al. 2002). It is intriguing to see how these tropical variations would project onto the extratropics by exciting planetary waves. In this context, aerosol impacts are initiated *indirectly*. This study explores the validity of this paradigm.

Some details helpful for understanding the results are provided here. Ming and Ramaswamy (2009) described the atmospheric GCM (AGCM) and its coupling with a slab (mixed layer) ocean model, and the design of the experiments examined in this study. The AGCM is based on the Geophysical Fluid Dynamics Laboratory (GFDL) Atmospheric Model version 2.1 (AM2.1; GFDL Global Atmospheric Model Development Team 2004), but modified to include a prognostic treatment of aerosol indirect effects (Ming et al. 2006, 2007). The climatological atmospheric burdens of sulfate, black carbon, organic carbon, and dust are generated by running a chemical transport model (Horowitz 2006), and thus do not interact with the GCM-simulated meteorology and climate. Sea salt within the marine boundary layer is parameterized as a function of
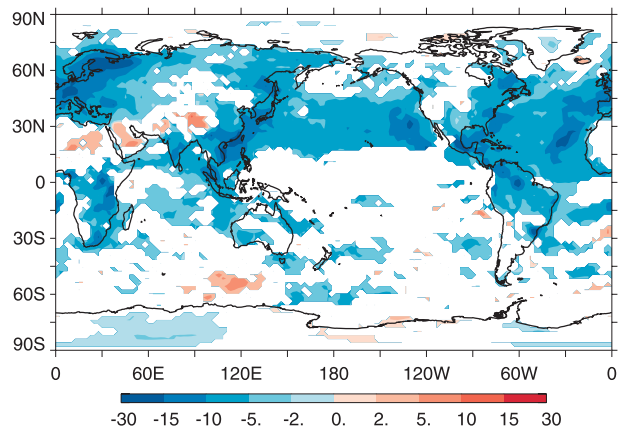

FIG. 1. Radiative flux perturbation of anthropogenic aerosols (W m^{-2}) (colored shading with statistical significance at the 95% confidence level).

satellite-retrieved surface wind speed (Haywood et al. 1999).

With all the climate forcings set at their 1860 values, the preindustrial control (CONT) simulation lasts 140 model years. Three perturbation cases are created from subjecting the control at the beginning of year 41 to present-day aerosols (AERO), to present-day radiatively active gases (GAS), and to aerosols and gases simultaneously (BOTH). Note that the term "present day" refers specifically to 1990 in this study. After reaching equilibrium after ~20 model years, each of the perturbation experiments is integrated for another 80 model years. The equilibrium responses and their statistical significance are computed from the last 80 years of the simulations.

The combined aerosol direct (by scattering/absorbing sunlight) and indirect (by altering cloud properties) effects can be quantified as radiative flux perturbation, which is the variation in the top-of-the-atmosphere radiative flux after the atmosphere adjusts to the presence of a climate forcing agent (Hansen et al. 2005; Haywood et al. 2009). In this model, the preindustrial to present-day increases of anthropogenic aerosols give rise to a global-mean radiative flux perturbation of −2.1 W m^{-2}, about 74% of which is a result of indirect effects. The geographical distribution is highly inhomogeneous, with some of the strongest forcing over the NH midlatitude source regions (e.g., East Asia, North America, and Europe) and over the oceans downwind of them (e.g., the North Pacific and North Atlantic; Fig. 1). The tropical aerosol forcing caused mainly by biomass burning is centered over the sources (e.g., central Africa, Amazon, South Asia, and Southeast Asia). In comparison, the instantaneous radiative forcing and radiative flux perturbation of radiatively active gases are 2.5 and 2.1 W m^{-2},

respectively. Despite the relatively small difference between them due to the atmospheric-only adjustment to gases, both forcing measures are distributed rather evenly over the entire globe.

We first discuss the changes in the boreal winter (December–February) extratropical zonal-mean and zonally asymmetrical flows (stationary eddies) caused by aerosols and gases (BOTH), while attributing them to specific forcing by comparing with the individual responses (AERO and GAS). Then, we examine how the altered time-mean flow may affect the transient eddy activity, and the meridional transport of moist static energy and moisture.

2. Zonal-mean flow

The zonal-mean change in potential temperature (θ) due to aerosols and gases (BOTH) is plotted in Fig. 2a. Some of the characteristics (e.g., enhanced warming in the tropical upper troposphere, polar amplification of warming, and stratospheric cooling) are clearly associated with GAS (Fig. 2c). Even though the negative aerosol forcing far outweighs the positive gas forcing over the NH midlatitude aerosol source regions (Fig. 1), the combined effect is only a mild surface cooling of a few tenths of a degree, hinting at mitigation of aerosol cooling by circulation adjustment. In the midlatitude troposphere, the cooling decreases gradually with altitude below ~400 hPa, while the gas-induced warming dominates above. This results in a decrease in lapse rate (Γ) and an increase in dry static stability. In contrast, the cooling is amplified in the upper troposphere in response to aerosols alone (AERO; Fig. 2b). As discussed in section 6, the stabilizing effect of gases outweighs the destabilization effect of aerosols.

The poleward shift of the SH subtropical jet and the equatorward shift of its NH counterpart are pronounced in Fig. 3a, which depicts the change in zonal wind (u) in BOTH. They are of different origins. The former is attributed to the gas-induced warming (Fig. 3c; e.g., Hall et al. 1994; Kushner et al. 2001; Yin 2005). As shown in Figs. 2a,b, the aerosol-induced cooling collocates approximately with the mean location of the NH jet. It strengthens the meridional temperature gradient on the equatorward side of the jet, while weakening it on the poleward side. According to the thermal–wind relationship, the westerlies accelerate in the former case, and decelerate in the latter, giving rise to a net equatorward displacement of the jet (Figs. 3a,b). This indicates that the local aerosol forcing is capable of reversing the warming-induced poleward shift. The surface winds display a similar equatorward shift that cannot be explained
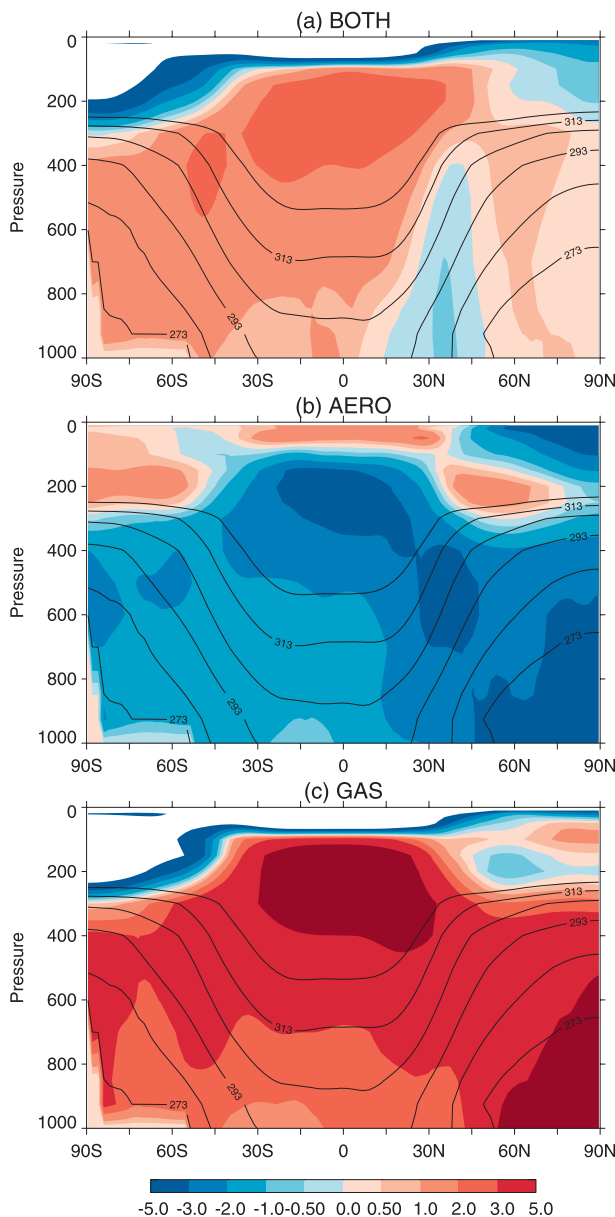

FIG. 2. Differences in zonal-mean θ (K) (the perturbation cases minus CONT; colored shading). The contour lines denote the climatological mean in CONT (between 273 and 323). The y axis is pressure (hPa).

by the thermal wind (not shown); it has to be related to the change in eddy momentum flux and associated mean meridional circulation. Note that this result does not agree with the observed poleward expansion of the Hadley circulation in both hemispheres (e.g., Fu et al. 2006; Hu and Fu 2007). The reasons are manifold. The equilibrium climate response discussed here by definition has not been fully realized in the real world. As aerosol forcing suffers from large uncertainties (e.g., Forster et al.
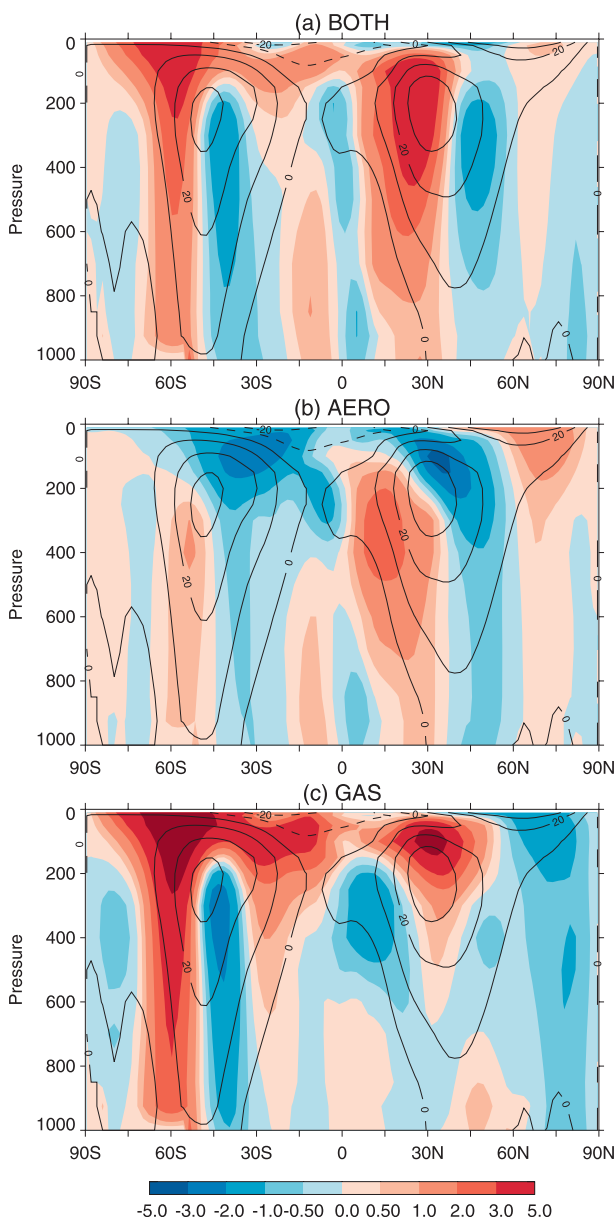
FIG. 4. Differences in tropopause height (hPa). Negative values indicate higher tropopause and vice versa.

FIG. 3. Differences in zonal-mean u (m s^{-1}) (the perturbation cases minus CONT; colored shading; westerlies as positive) at different pressure levels (hPa). The contour lines denote the climatological mean in CONT (between -20 and 30 m s^{-1}). The y axis is pressure (hPa).

2007), its magnitude and impact on the location of the NH subtropical jet may have been exaggerated in this study. Moreover, climate models generally have difficulties in capturing the full extent of the observed expansion (Johanson and Fu 2009). The model used here may have the same deficiency.

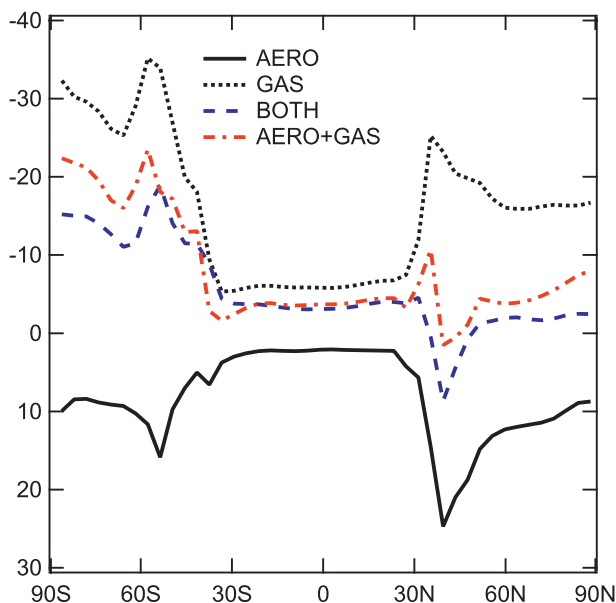By computing the lapse rate linearly with pressure between model layers (Reichler et al. 2003), we estimate the tropopause height from the vertical temperature profile as the lowest pressure level at which the lapse rate drops below 2 K km^{-1} (World Meteorological Organization 1957). The tropopause rises almost uniformly by 3–4 hPa between 30°S and 30°N in BOTH (Fig. 4). The rise is even greater (more than 10 hPa) in the SH extratropics, thus lessening the downward slope of the tropopause. In contrast, the NH extratropical tropopause generally rises only by ~2 hPa, leaving the local slope little changed. One can understand the different hemispheric responses from the individual responses simulated in AERO and GAS. For aerosols, the lowering of the troposphere occurs at all the latitudes, but is more pronounced in the extratropics than in the tropics. The precipitous drop at ~40°N coincides with the equatorward shift of the NH subtropical jet, as the jet roughly divides the tropics (with higher tropopause) and extratropics. Conversely, the poleward shift of the subtropical jets associated with warming has a tendency of elevating the tropopause in both hemispheres. It is clear from Fig. 4 that the two opposite effects are roughly linear in the tropics, but not so in the extratropics (especially in the NH extratropics), an important point to which we shall return in section 6. They largely offset each other in the tropics and NH extratropics, while the gas effect dominates in the SH extratropics.

3. Zonally asymmetrical flow

The longitudinal variations in the Earth's climate arise from zonally asymmetrical boundary conditions such as

topography and the land–sea contrast in diabatic heating, which are capable of exciting stationary Rossby waves (Held et al. 2002). From the viewpoint of climate change, a change in diabatic heating can alter stationary wave patterns, and thus affect regional climate. Another potential source of zonal asymmetry in the context of climate change is inhomogeneous forcing. This is particularly true of aerosols. These two factors are often intertwined, and may not be separated cleanly.

The change in surface temperature (T_s) caused by aerosols and gases has rich spatial structures (Fig. 5a). The aerosol cooling occurs mostly in the NH midlatitudes, but varies within the latitudinal band. Of particular interest is that the cooling appears to organize tightly into an elongated region approximately along the North Pacific storm track, but is much more scattered over the North Atlantic, despite similar distributions of aerosol forcing over two oceans (Fig. 1). This pattern is also present in AERO (Fig. 5b). (We will discuss the cause of this distinction later in this section.) This explains why the equatorward shift of the NH subtropical jet seen in the zonal-mean flow takes place preferentially over the North Pacific (Figs. 6a,b). Besides, the strong warming over parts of northernmost Eurasia and North America lies immediately north of the North Pacific cooling, giving rise to a substantial reduction in the local meridional temperature gradient, and further decelerating the poleward flank of the jet. In contrast, the SH extratropical warming and accompanying poleward shift of the jet in BOTH are fairly uniform across the latitudinal band (Figs. 5a and 6a), consistent with GAS (Figs. 5c and 6c). Note that the tropical Pacific warming in BOTH is El Niño–like (i.e., the warming over the east Pacific is greater than over the west Pacific), a pattern common to the GCM-simulated response to global warming (Vecchi et al. 2008).

The lower pressure over the entire extratropical North Pacific is characteristic of the change in sea level pressure (SLP) caused by aerosols and gases, and constitutes a southeastward shift of the Aleutian low (Fig. 7a). This is in sharp contrast with the generally higher pressure over the North Atlantic–European sector. These circulation changes are barotropic as they are also present over the same regions in the changes in 500-hPa geopotential height (Z) (Fig. 8a) and in 300-hPa stationary eddy streamfunction (Ψ) (Fig. 9a). A comparison with the individual responses [panels (b) and (c) in Figs. 7–9] yields that these characteristics are broadly consistent with AERO, instead of GAS, indicating that they are attributable to anthropogenic aerosols. Note that the pattern of a trough over the North Pacific and a ridge over North America in the combined response resembles the classic Pacific–North America (PNA) teleconnection
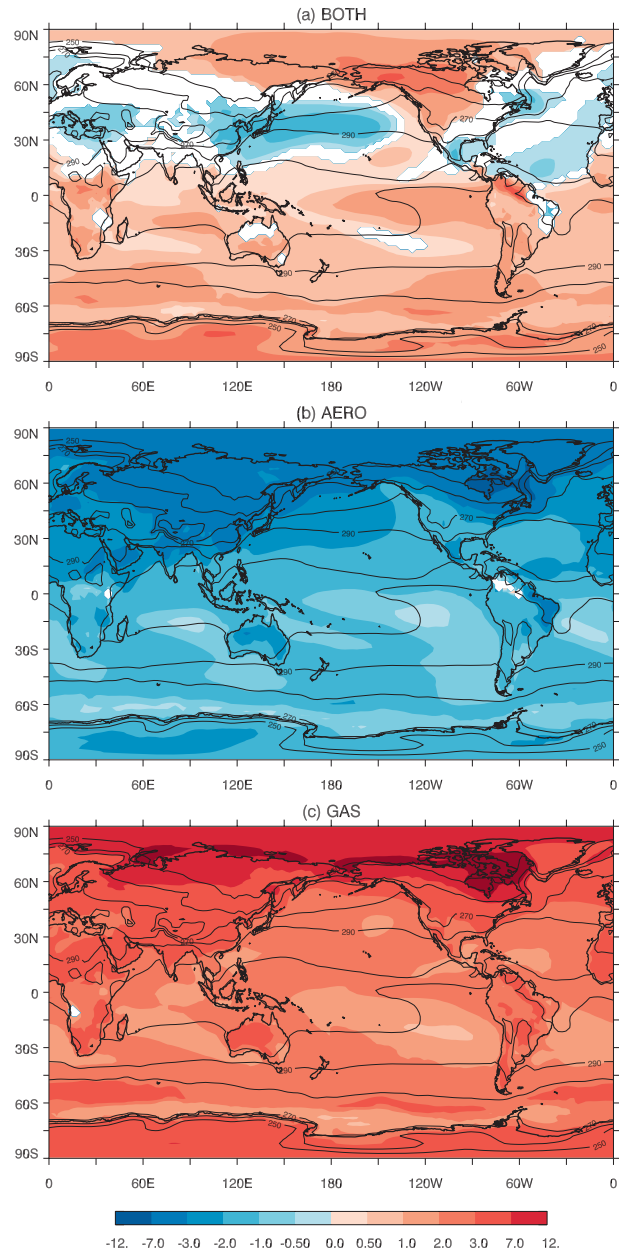

FIG. 5. Differences in T_s (K) (BOTH minus CONT; colored shading with statistical significance at the 95% confidence level). The contour lines denote the climatological mean in CONT (between 250 and 300 K).

response to El Niño (see Fig. 2a of Lau 1997). In light of the El Niño–like tropical Pacific warming as discussed above, it is tempting to contemplate the link between the east Pacific oceanic state and the extratropical circulation.

An observation is that the change in the stationary eddy streamfunction is wavelike (Fig. 9a). (This is not nearly as evident for Z, particularly in the tropics, as $Z \propto f \Psi$. f is the Coriolis parameter.) Note that zonally
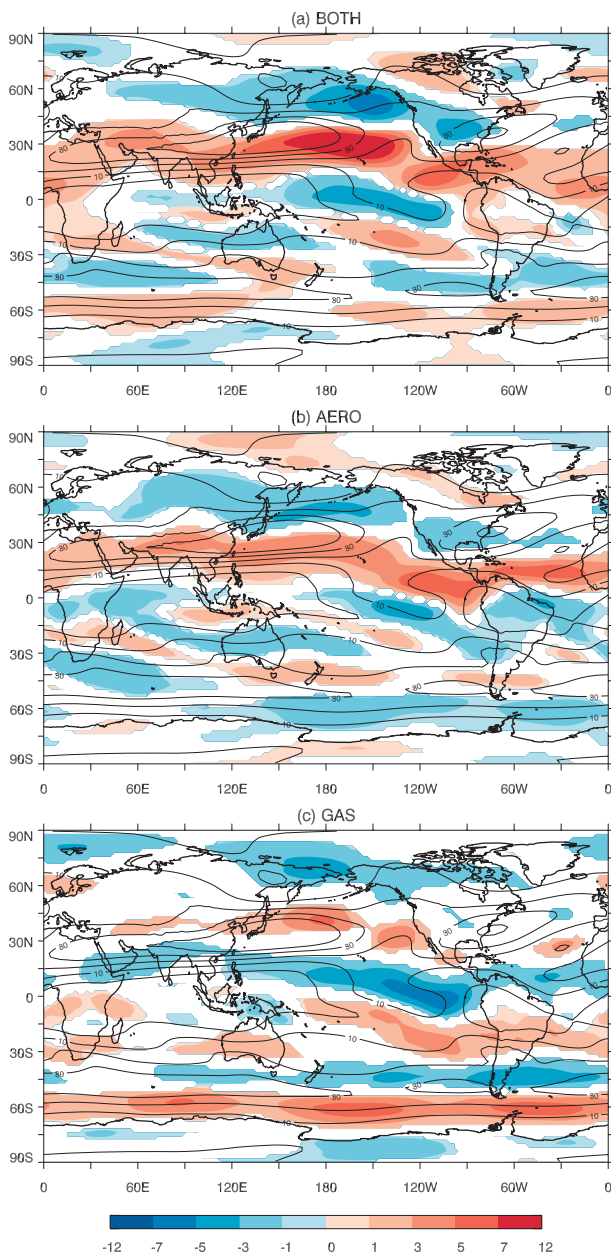
FIG. 6. Differences in 300-hPa u (m s^{-1}) (the perturbation cases minus CONT; colored shading with statistical significance at the 95% confidence level; westerlies as positive). The contour lines denote the climatological mean in CONT (between 0 and 40 m s^{-1}).
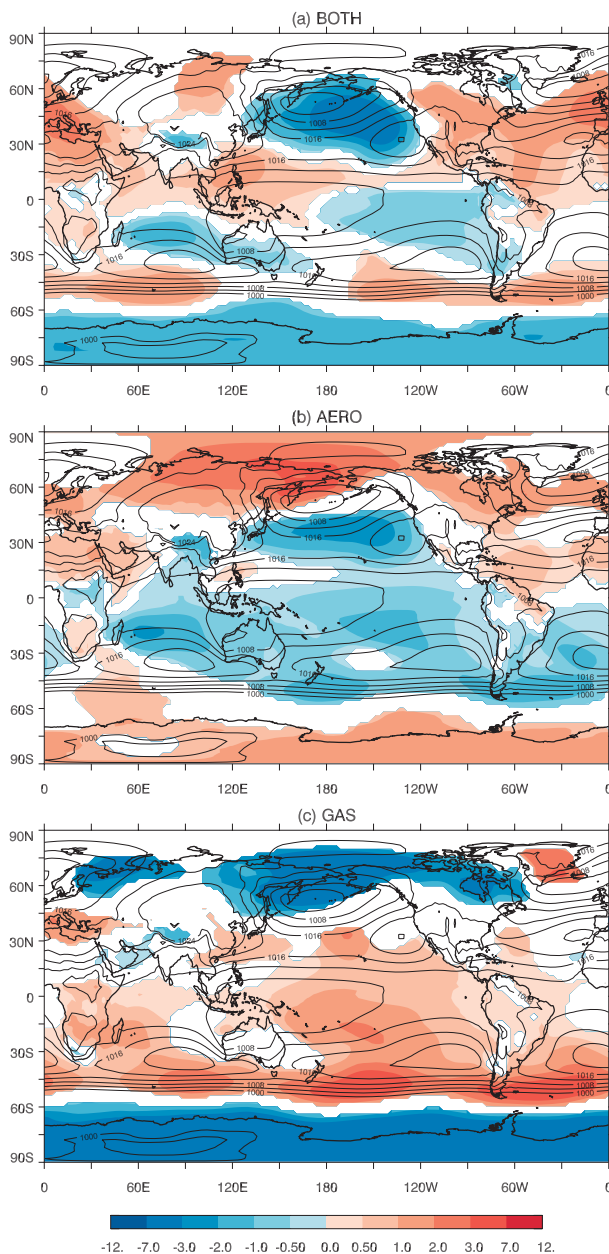

FIG. 7. Differences in SLP (hPa) (BOTH minus CONT; colored shading with statistical significance at the 95% confidence level). The contour lines denote the climatological mean in CONT (between 1000 and 1024 hPa).

asymmetrical diabatic heating is a main source of stationary Rossby waves (Held et al. 2002). Figure 10a shows the change in precipitation (P), which can be viewed roughly as a proxy for diabatic heating, in response to aerosols and gases. It features a substantial reduction in precipitation north of the equator and an increase of comparable magnitude to the south. Because this overall pattern resembles that of AERO (Fig. 10b), but is missing

from GAS (Fig. 10c), one can attribute it to the former. In fact, this southward shift of rainfall is a reasonably robust hydrological response to aerosols across different models (Williams et al. 2001; Rotstayn and Lohmann 2002; Feichter et al. 2004; Krisjánsson et al. 2005). As explained in Ming and Ramaswamy (2011), the tropical circulation adjustment to aerosols is driven fundamentally by the need to lessen the energy imbalance between
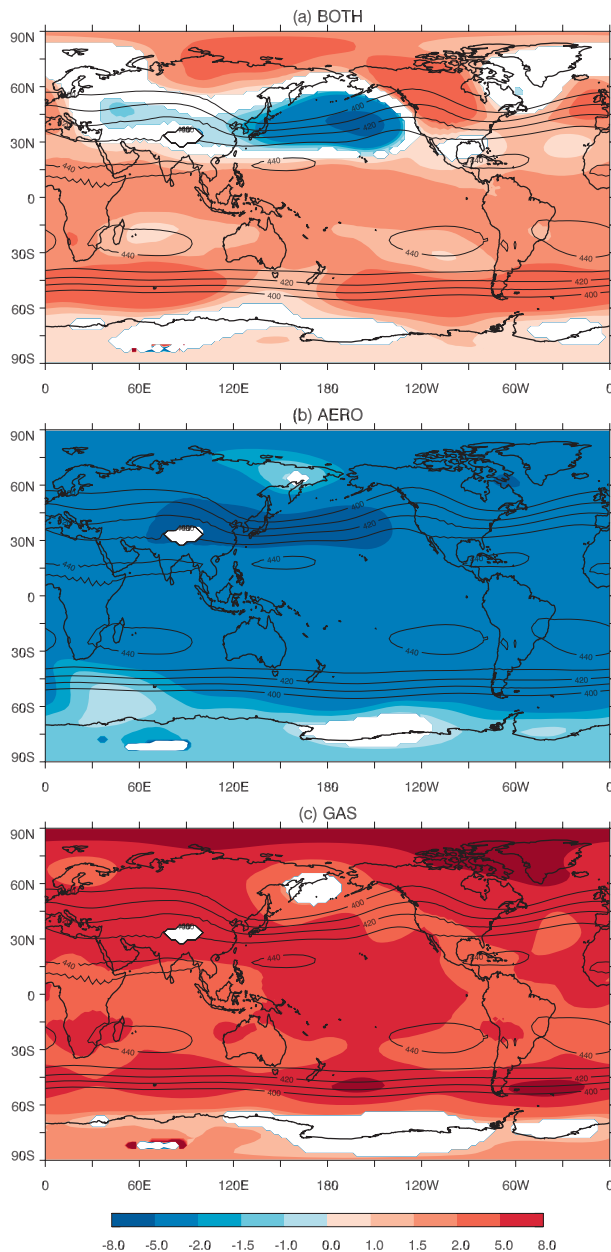
FIG. 8. Differences in 500-hPa Z (10 m) (the perturbation cases minus CONT; colored shading with statistical significance at the 95% confidence level). The contour lines denote the climatological mean in CONT (10 m) (between 4000 and 4400 m).

FIG. 9. Differences in 300-hPa stationary eddy streamfunction (10^6 m^2 s^{-1}) (the perturbation cases minus CONT; colored shading; clockwise circulations as positive). The contour lines denote the climatological mean in CONT (10^6 m^2 s^{-1}) (between -1.5×10^7 and 1.5×10^7 m^2 s^{-1}).

NH and SH. Although the change in rainfall implies more latent energy being transported from NH to SH, this effect is not strong enough to reverse the enhanced export of dry static energy in the opposite direction. The net northward cross-equatorial moist static energy flux compensates for the radiative deficit posed by aerosols in the NH (see section 5). In the extratropics, the precipitation associated with the North Pacific storm track
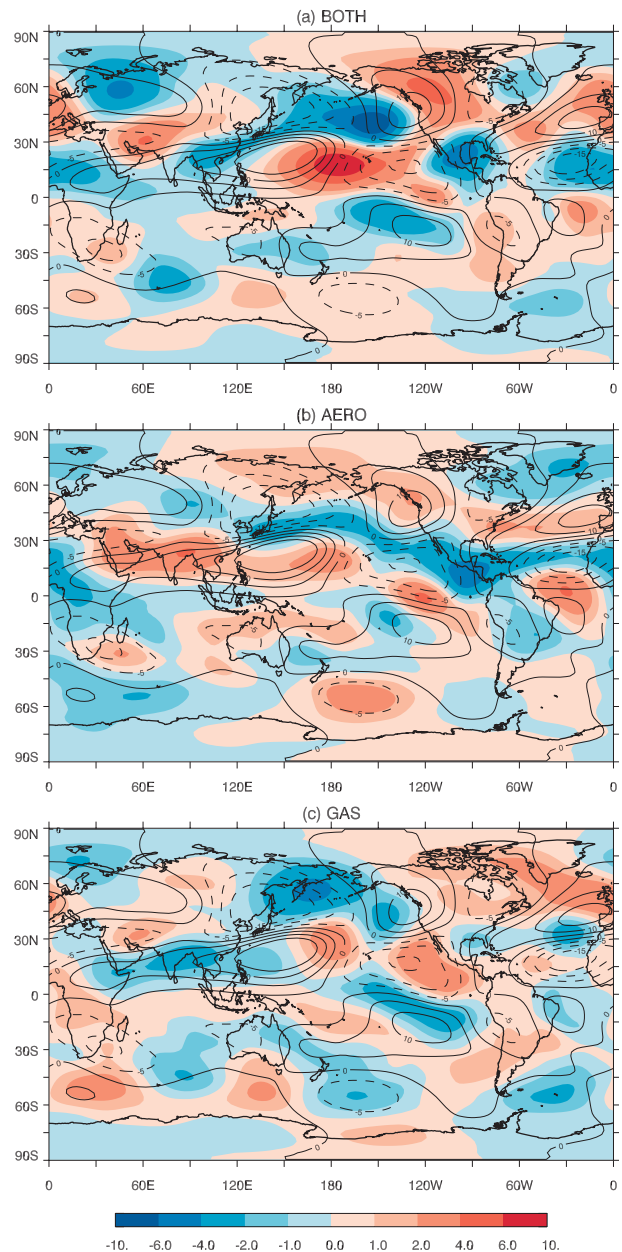
shows a southeastward shift, consistent with the change in SLP (Fig. 7a). One wonders how the change in diabatic heating, with its complex spatial structures, would affect wave pattern and circulation.

We answer this question with a set of idealized model experiments, which are described in the appendix. It is reassuring to see that the idealized model, when being forced by the GCM-simulated diabatic heating in
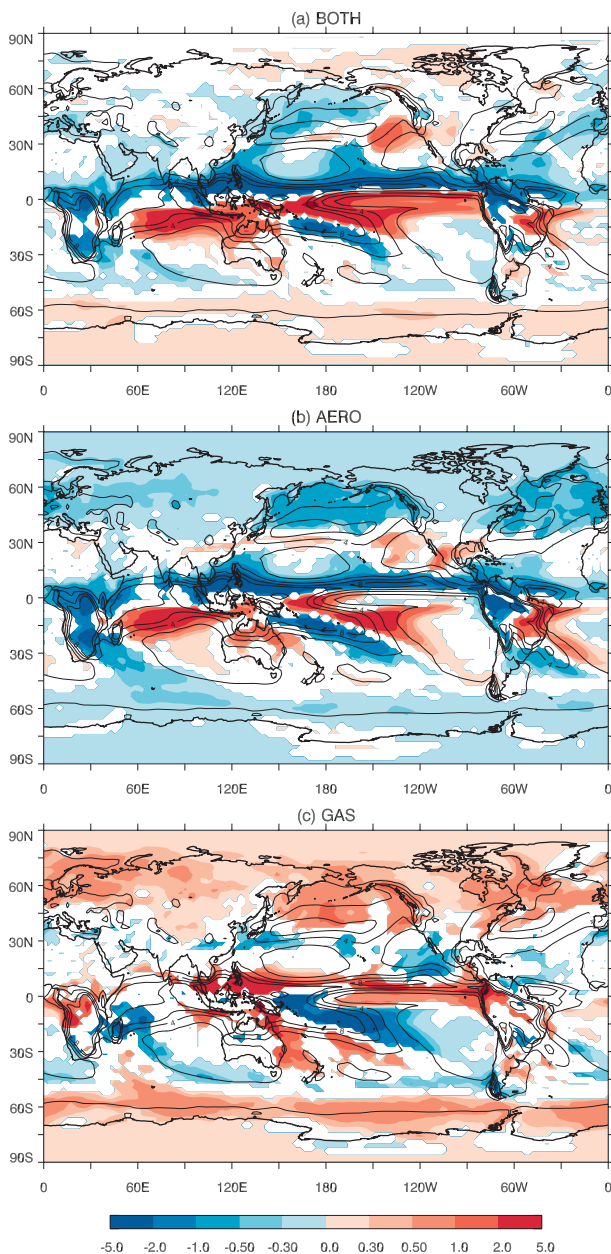
FIG. 10. Differences in P (mm day^{-1}) (the perturbation cases minus CONT; colored shading with statistical significance at the 95% confidence level). The contour lines denote the climatological mean in CONT (between 0 and 22 mm day^{-1}).

CONT or in BOTH, can capture reasonably well the main characteristics of the stationary eddy climatology and the response to the difference in heating simulated with the full GCM (Fig. 11a). An example is the PNA pattern discussed above. This demonstrates the model's utility for interpreting the full GCM simulations. We are able to decompose the total response into those forced by the differences in diabatic heating over three regions: the tropical Indian Ocean and west Pacific (30°S–30°N,

0°–150°E), the tropical east Pacific and Atlantic (30°S–30°N, 150°E–0°), and the extratropical North Pacific and North Atlantic (north of 30°N; Figs. 11b–d). Note that the simulated total response (Fig. 11a) is grossly similar to the linear sum of the three individual responses (Fig. 11e).

In Fig. 11b, a wave train emanates from the tropical Indian Ocean and west Pacific into the NH midlatitudes. It then turns around over the North Pole, with the tilt changing from northwest–southeast (NW–SE) to northeast–southwest (NE–SW), before being absorbed by the tropics over the Pacific. A cyclone forms over the North Pacific (~30°–60°N) along with an anticyclone to its southeast over the tropical Pacific (~15°–30°N). The wave source over the tropical east Pacific is evident in Fig. 11c. The northward propagation with NW–SE tilt is associated with a cyclone centered at ~30°N over the Pacific and a pronounced anticyclone over North America, which constitute a PNA-like pattern. The extratropical heating excites a wave train with NE–SW tilt, leading to a cyclone approximately at 30°–50°N over the North Pacific (Fig. 11d). Thus, we conclude that the midlatitude circulation change is driven mainly by the heating anomaly over the tropical east Pacific, as opposed to that over the tropical Indian Ocean and west Pacific. This finding is consistent with the previous studies of the influence of El Niño on the extratropical circulation (e.g., Lau 1997). Despite this apparent similarity, one has to note that the wave train is typically forced by a longitudinal shift of heating from the west Pacific to the east Pacific in a real El Niño event. Here, when all the heating sources are considered, the shift is mainly in the latitudinal direction. The latter shift is more symmetrical in the zonal direction than the former, and thus is less efficient at exciting stationary Rossby waves.

We return to the question of why the spatial distributions of the temperature change are so different over the two oceans: the aerosol-induced cooling is much more concentrated over the North Pacific between ~30°–60°N than over the North Atlantic. As discussed above, the change in tropical diabatic heating strongly modulates the time-mean flow over the North Pacific by exciting stationary Rossby waves, while leaving the North Atlantic largely unaffected. The large change in the zonal wind over the North Pacific can be achieved only by maintaining strong local meridional temperature gradients. This is an important contributing factor to the zonally asymmetrical climate response.

4. Transient eddies

As an effective means of transporting energy and momentum, baroclinic eddies play important roles in driving the general circulation and hydrological cycle. In
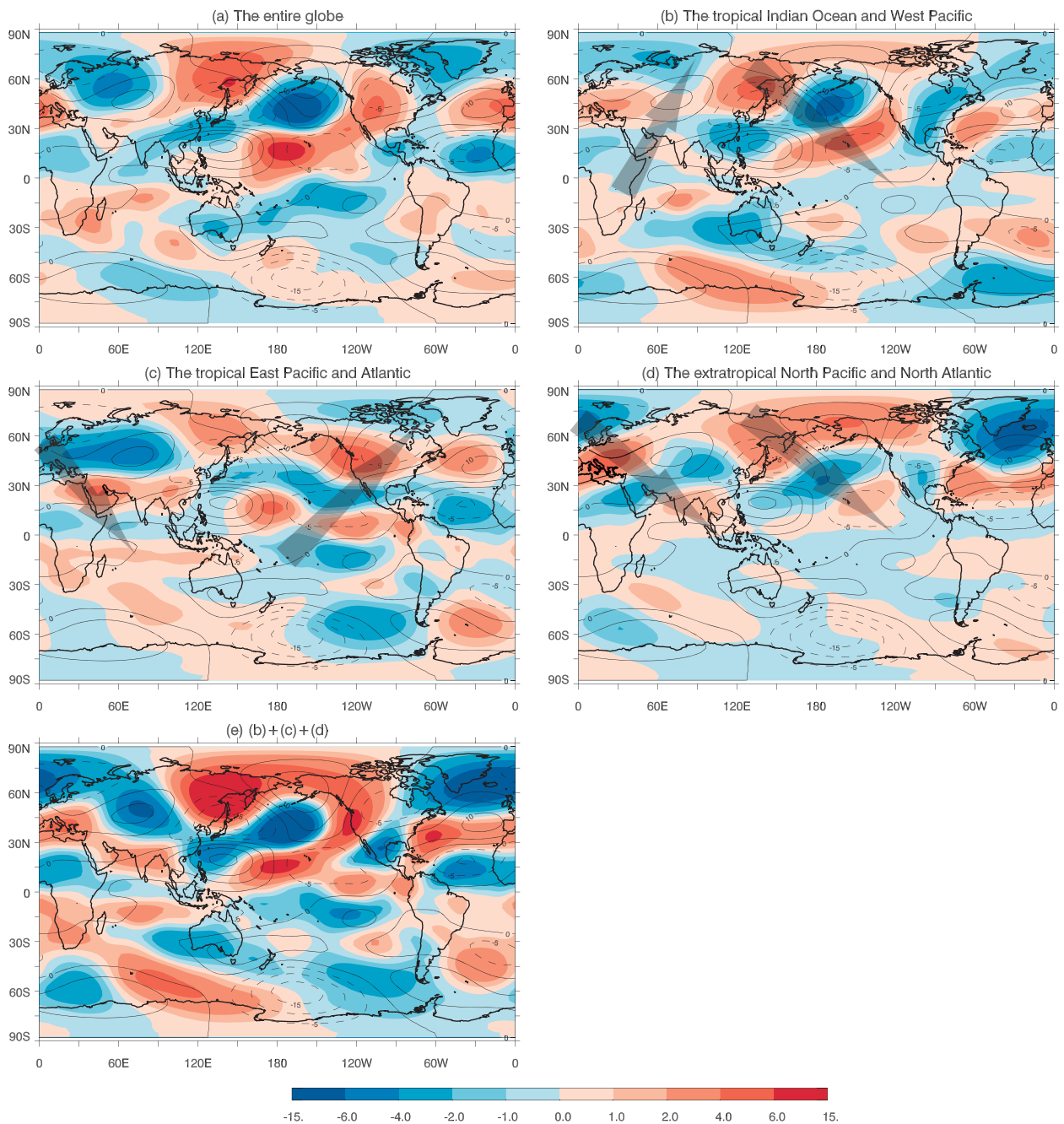
FIG. 11. Differences in 300-hPa stationary eddy streamfunction (10^6 m^2 s^{-1}) (colored shading; clockwise circulations as positive) simulated with the idealized model in response to the differences in diabatic heating between CONT and BOTH (a) over the entire globe, (b) over the tropical Indian Ocean and west Pacific (30°S–30°N, 0°–150°E), (c) over the tropical east Pacific and Atlantic (30°S–30°N, 150°E–0°), and (d) over the extratropical North Pacific and North Atlantic (north of 30°N). (e) The linear sum of (b),(c), and (d). The contour lines denote the climatological mean in the control case (10^6 m^2 s^{-1}) (between -1.5×10^7 and 1.5×10^7 m^2 s^{-1}). The gray arrows sketch the directions in which the stationary Rossby waves propagate.

response to aerosols and gases, a substantial reduction in 300-hPa transient eddy kinetic energy occurs over the North Pacific, and extends downstream into North America (Fig. 12a). The less energetic eddies and lower

temperature (less moisture; Fig. 5a) contribute to a suppression of precipitation on the poleward side of the Pacific storm track (Fig. 10a). One can relate the production of baroclinic eddies to the state of the time-mean
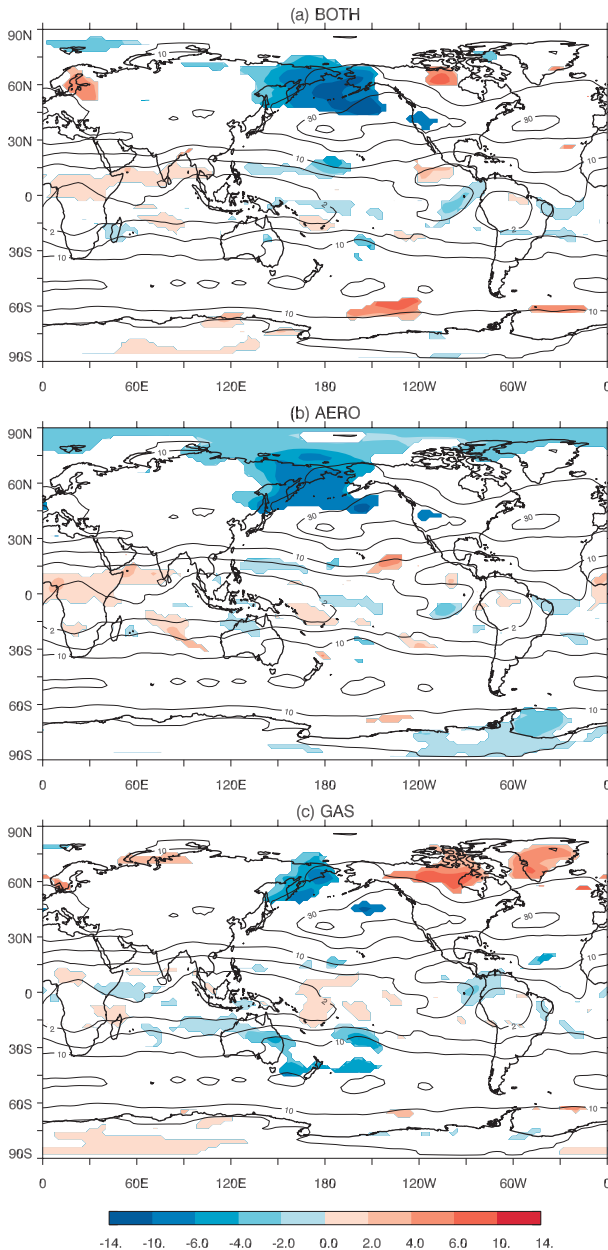
FIG. 12. Differences in 300-hPa transient eddy kinetic energy (10 m^2 s^{-2}) (the perturbation cases minus CONT; colored shading with statistical significance at the 95% confidence level). The contour lines denote the climatological mean in CONT (10 m^2 s^{-2}) (between 20 and 400 m^2 s^{-2}).
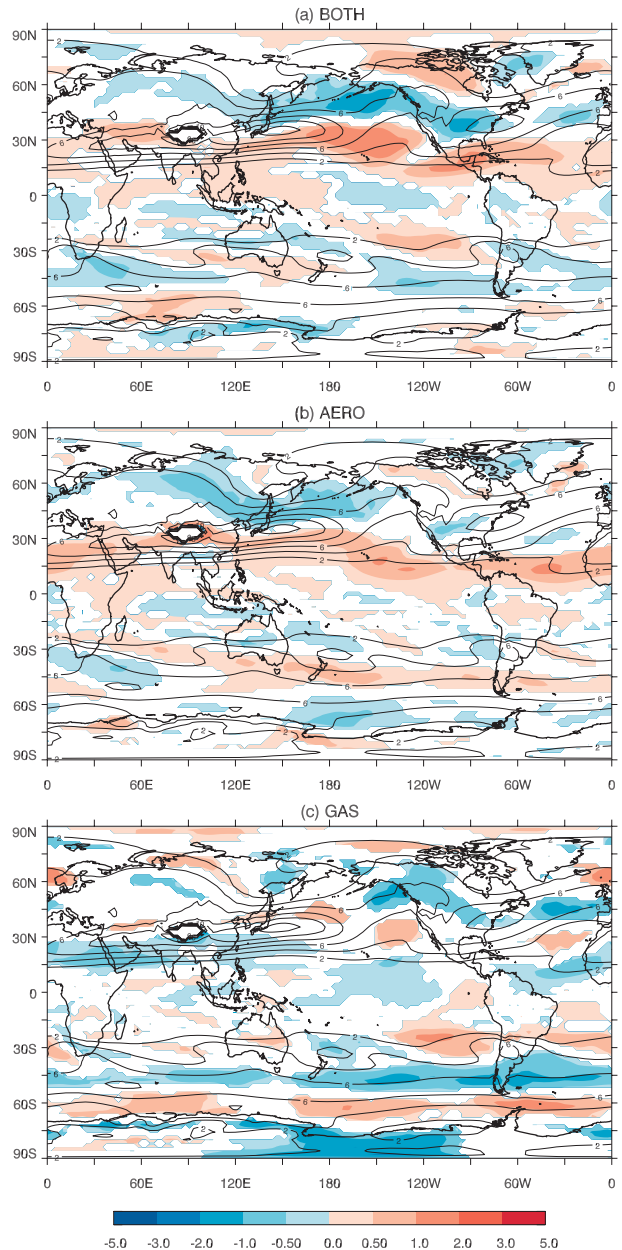
FIG. 13. Differences in 500-hPa maximum Eady growth rate (10^{-1} day^{-1}) (the perturbation cases minus CONT; colored shading with statistical significance at the 95% confidence level). The contour lines denote the climatological mean in CONT (10^{-1} day^{-1}) (between 0.2 and 1.2 day^{-1}).

flow with the maximum Eady growth rate (σ_{BI}) (Lindzen and Farrell 1980; Hoskins and Valdes 1990). It is defined as $0.31(f/N)|\partial\mathbf{v}/\partial z|$, where N is the Brunt–Väisälä frequency, $\mathbf{v}$ is the horizontal wind vector, and z is the geometric height. The σ_{BI} at 500 hPa shows a pronounced decrease over the North Pacific (Fig. 13a), a pattern broadly consistent with the difference in eddy

kinetic energy. A further analysis indicates that $\delta\sigma_{BI}$ arises mainly from the change in vertical wind shear, which is tied to the change in the local meridional temperature gradient caused by the concentrated aerosol cooling (Fig. 5a), while the dry static stability, and thus N are little changed in the middle troposphere (Fig. 2). This argument is consistent with the fact that weaker
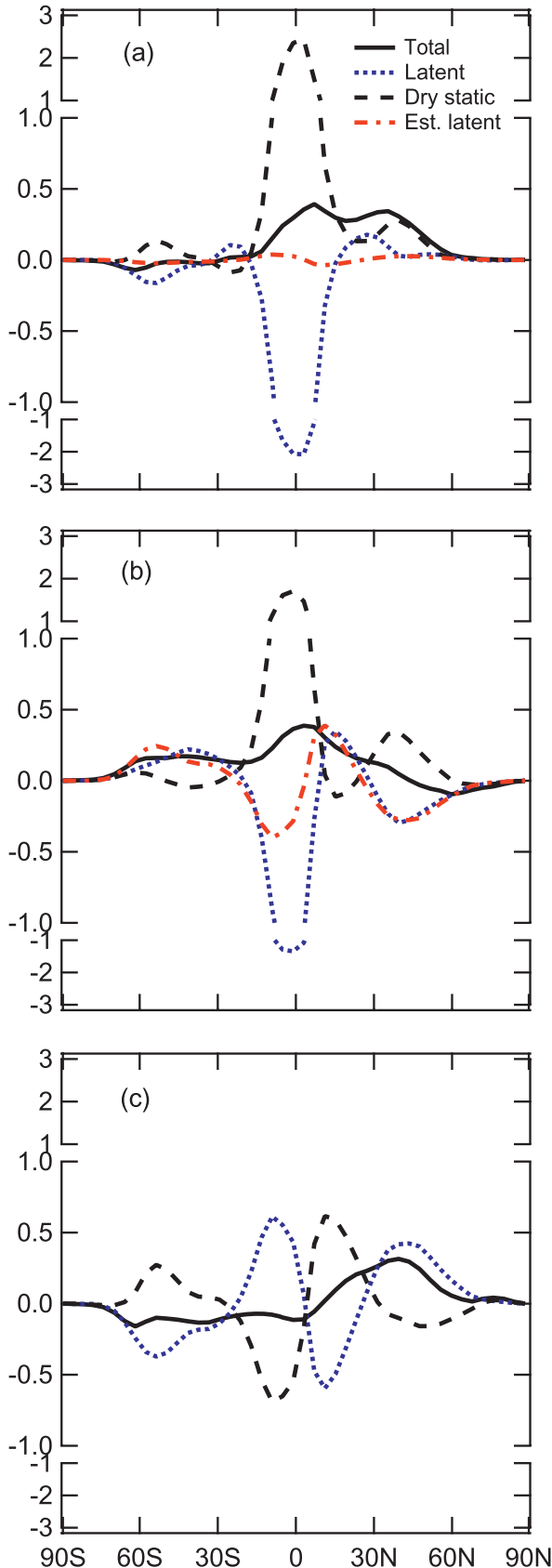
transient eddies and slower Eady growth rates also take place in AERO, but not in GAS [panels (b) and (c) in Figs. 12–13]. Lorenz and DeWeaver (2007) reported large increases in the annual average zonal-mean eddy kinetic energy on the poleward sides of the storm tracks owing to strong CO_2-induced warming. That finding does not contradict the aerosol effects discussed here.

5. Atmospheric moist static energy transport

One may attempt to understand the collective climate impacts of the detailed circulation changes by examining the variations in the atmospheric transport of energy and moisture. As explained in Ming and Ramaswamy (2011), the interhemispheric asymmetry in aerosol forcing leads to a net cross-equatorial moist static energy flux from the SH to the NH through strengthening the boreal winter Hadley circulation (Fig. 14b). This supply of energy is deposited mainly between 0°–60°N, where most aerosol forcing is located. A cross-equatorial flux of similar magnitude is also present in BOTH (Fig. 14a), suggesting that this phenomenon has its root in the aerosol-induced tropical circulation adjustment. As shown in Fig. 15, the overall shape of the change in the total atmospheric energy transport (δF) is similar to that of the linear sum of the individual responses.

Because of the strong dependence of the saturated water vapor pressure on temperature (the Clausius–Clapeyron scaling), the warming-induced change in latent heat transport (δF_L) is thermodynamically controlled to the first order (i.e., proportional to δT_s; Held and Soden 2006). To test to what extent this argument holds for aerosols, we estimate δF_L for AERO or BOTH by scaling the actual δF_L for GAS with the global-mean δT_s in each case. For example, $\delta F_{L,AERO}$ can be calculated as $\delta F_{L,GAS}\delta T_{s,AERO}/\delta T_{s,GAS}$. The agreement between the simulated and estimated δF_L is excellent in the extratropics, indicating that it is still valid to assume the thermodynamic control of δF_L. The results are somewhat surprising given that aerosols are rather potent at altering regional circulations, and once again reminds one how strongly the Clausius–Clapeyron scaling controls the hydrological response.

The changes in latent heat and dry static energy transport (δF_D) in response to global warming are often of opposite signs (e.g., Manabe and Wetherald 1975; Held and Soden 2006). This is true not only for GAS

←

FIG. 14. Differences in zonal-mean northward atmospheric energy transport (PW) (a) the perturbation cases minus CONT, (b) AERO minus CONT, and (c) GAS minus CONT.
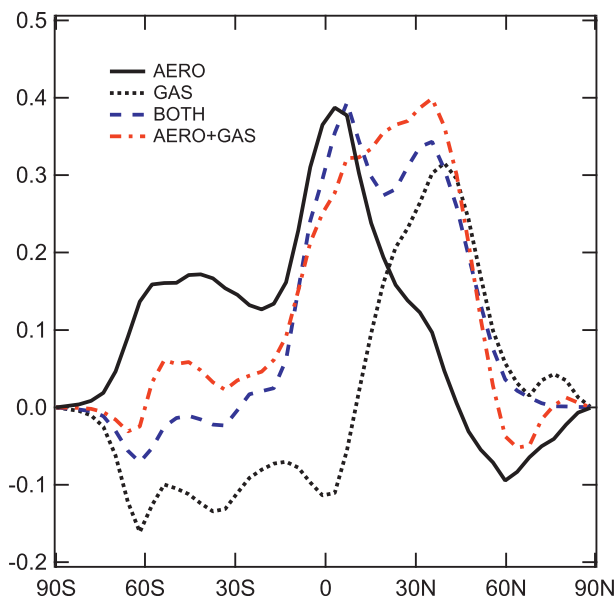
FIG. 15. Differences in zonal-mean northward atmospheric heat transport (PW) (northward as positive).

FIG. 16. Differences in zonal-mean surface temperature (K).

(Fig. 14c), but also for AERO (Fig. 14b). The difference is that decreased F_D cancels out part of increased F_L in the extratropics in the former case, while decreased F_L compensates for a large fraction of increased F_D in the latter. For BOTH, F_L is almost negligible north of ~40°N as a result of small temperature change. The increase in atmospheric energy transport is realized mainly by enhanced F_D. It would be of interest to investigate whether these characteristics specific to aerosols are present in fully coupled atmosphere–ocean general circulation models (AOGCMs) in light of the potentially important role of oceanic energy transport (Held and Soden 2006).

6. Nonlinear thermal response

The simulated surface temperature change in response to aerosols and gases deviates from the linear sum of the individual responses in the NH (Fig. 16), an issue highlighted in Ming and Ramaswamy (2009). Particularly intriguing is the small yet robust nonlinearity in the low and midlatitudes, where the surface albedo feedback is absent, and thus can be ruled out as cause of the nonlinearity. It is also reflected in the change in 300-hPa zonal-mean u (Fig. 17). The NH subtropical jet undergoes a distinct equatorward shift in AERO, while moving poleward in GAS. The linear sum of AERO and GAS captures the overall pattern of wind change in BOTH (i.e., an equatorward displacement that is less pronounced than in AERO), but significantly underestimates the acceleration on the equatorward flank of the jet.
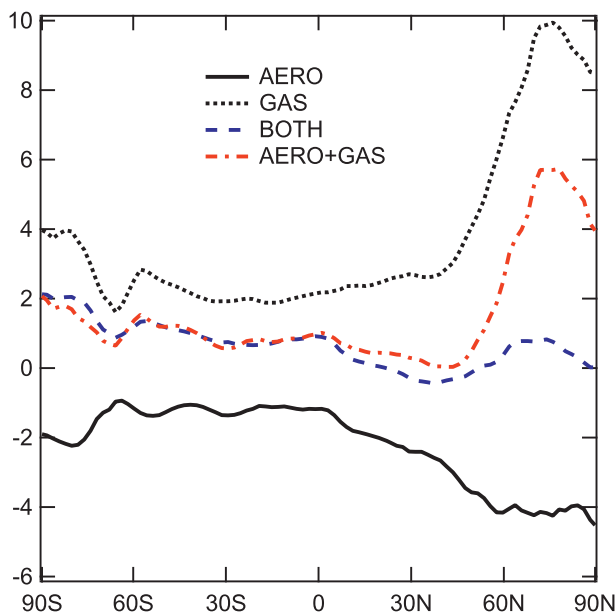
One can relate the mean location of the jet to baroclinic instability (C) using the Phillips (1954) criterion, which states $C \propto u_z/\theta_z$ with $u_z = u_{500} - u_{850}$ and $\theta_z = \theta_{500} - \theta_{850}$. The subscripts denote the pressure levels (in hPa) at which u and θ are evaluated. Lu et al. (2008) utilized this criterion to study the poleward jet shift and expansion of the Hadley circulation associated with global warming. The changes in u_z and θ_z between 10°–35°N,
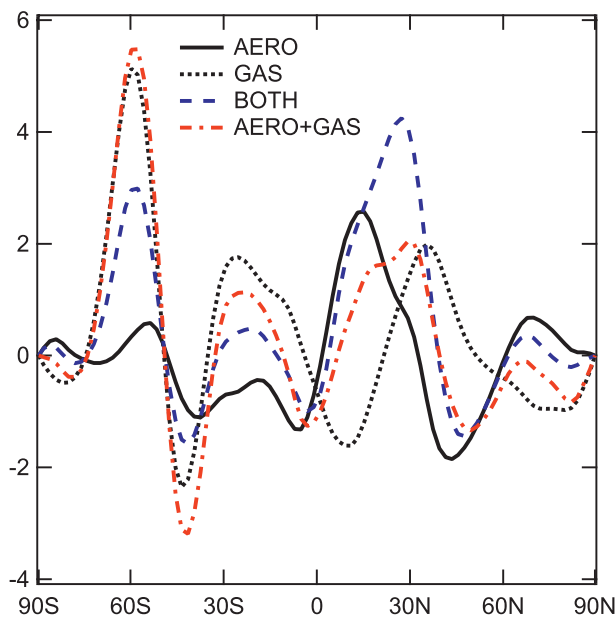

FIG. 17. Differences in zonal-mean 300-hPa u (m s^{-1}) (westerlies as positive).

TABLE 1. Mean differences in u_z and θ_z between 10°–35°N.

	δu_z (m s^{-1})	$\delta\theta_z$ (K)	$\delta u_z/u_z$ (%)	$\delta\theta_z/\theta_z$ (%)	$\delta C/C$ (%)
AERO	1.2	−0.63	8.3	−2.7	11.0
GAS	−0.27	2.08	−1.9	7.8	−9.7
BOTH	1.5	1.1	10.6	4.5	6.1
AERO + GAS	0.92	1.4	3.2	2.8	0.4

where the eddy momentum flux divergence is crucial for forming the descending branch of the Hadley circulation, are listed in Table 1. The warming caused by gases decreases slightly the vertical wind shear, while having a strong stabilizing effect on the thermal structure of the troposphere (i.e., weaker Γ) owing to moist convective adjustment and increased longwave absorption. In contrast, the aerosol cooling leads to a substantial increase in wind shear as a result of stronger meridional temperature gradients, and a small decrease in dry static stability. A comparison of BOTH with the linear sum of AERO and GAS suggests that $\delta\theta_z$ is approximately linear, but δu_z behaves nonlinearly. Since δu_z is approximately proportional to the meridional temperature gradient (i.e., the thermal wind relationship), the nonlinearity in δu_z is consistent with the nonlinear thermal response discussed above. Because $\delta C/C = \delta u_z/u_z - \delta\theta_z/\theta_z$, the effects of δu_z and $\delta\theta_z$ on C can be separated in terms of fractional changes (Table 1). Aerosols increase baroclinic instability mainly by enhancing wind shear, thus causing the tropical poleward flow to descend at a lower latitude and an equatorward shift of the jet, while gases decrease it mainly by stabilizing the troposphere, thus resulting in a poleward shift. If δu_z and $\delta\theta_z$ both behave linearly, the two opposite effects would largely cancel out, and leave the location of the jet unchanged, an outcome that obviously does not materialize in BOTH. Instead, the simulated meridional temperature gradient is stronger than suggested by the linear sum. The resulting net increase in baroclinic instability is consistent with the simulated equatorward shift of the jet. Note that the above argument is framed in the context of subtropical static stability and baroclinic instability (e.g., Frierson et al. 2007; Lu et al. 2008). It could be beneficial to approach the same issue from other angles such as near-tropopause meridional temperature gradient (e.g., Chen and Held 2007; Chen et al. 2008).

An inspection of the change in tropopause height (Fig. 4) yields a clue to the root cause of the nonlinearity. The linear sum indicates that the equatorward flank of the NH jet would move poleward (as the gas effect dominates locally), while the poleward flank would move in the opposite direction (i.e., equatorward) owing to the aerosol effect. The net effects are a *narrowing* of the jet

stream and a deformation of the curvature of the tropopause, which we theorize may be dynamically unstable as a narrower jet can affect barotropic instability (James 1987). As a consequence, both flanks prefer to move in the same direction with the latitudinal span of the jet little changed, thus leading to a deviation from the linear sum.

7. Conclusions

Maximum aerosol forcing is centered over the NH low and midlatitudes. During the boreal winter, the strong local aerosol forcing influences many of the key characteristics of the vigorous extratropical circulation by causing local cooling mainly over the source regions. Such a cooling enhances the meridional temperature gradient equatorward of the NH subtropical jet, but weakens it poleward. The end result is an equatorward shift of the jet.

The cooling over the North Atlantic is much more diffuse than over the North Pacific despite similar local forcings. A series of idealized model experiments show that the stationary Rossby waves excited by the anomalous diabatic heating over the tropical east Pacific, when propagating into the NH midlatitudes, cause a strong trough over the North Pacific. The low pressure anomaly results in a southeastward displacement of the Aleutian low, which is accompanied by an equatorward movement in the time-mean location of the North Pacifc subtropical jet and storm track. The associated acceleration of westerlies on the equatorward flank of the jet and deceleration on the poleward flank are consistent with the concentrated cooling over the North Pacific according to the thermal–wind relationship. The impacts of the heating anomalies over the tropical Indian Ocean and west Pacific and over the extratropical North Pacific and North Atlantic are secondary. This is consistent with the observation that the tropical Pacific warming and the midlatitude circulation changes are both El Niño–like in the simulations. The overall pattern of decreased precipitation north of the equator and increased precipitation south is robust across models (Williams et al. 2001; Rotstayn and Lohmann 2002; Feichter et al. 2004; Krisjánsson et al. 2005; Ming and Ramaswamy 2009). However, the regional response over a specific ocean may be less so. This shows the importance of understanding the detailed spatial pattern of the aerosol-induced tropical circulation change, which plays a critical role in determining the extratropical response by altering stationary Rossby waves.

One can understand the change in atmospheric energy transport by recognizing a few key attributes. A net energy influx into the NH low and midlatitudes acts to

alleviate local aerosol cooling. The zonal-mean meridional latent heat transport is firmly controlled by the thermodynamic scaling in the NH extratropics, even in the presence of large circulation changes caused by aerosols. This implies that one can predict reliably the changes in zonal-mean precipitation from the global-mean temperature change driven by aerosols and gases without a detailed knowledge of the concurrent circulation changes. On the other hand, the aerosol-induced zonally asymmetrical circulation changes are key to understanding the regional variations in precipitation.

We conclude by emphasizing the fact that the results presented in this paper are based on the simulations performed with a single climate model. It remains to be seen whether the detailed circulation changes discussed here are robust across different models.

APPENDIX

Description of Idealized Model Experiments

The atmospheric model is a standard hydrostatic spectral dynamical core forced with the boreal winter diabatic heating derived from the full GCM simulations (namely CONT and BOTH). The vertical differencing follows Simmons and Burridge (1981). Time stepping is realized with a semi-implicit leapfrog scheme with a Robert–Asselin time filter. The model is run with a horizontal resolution of T42 and 20 evenly spaced σ layers. The three-dimensional diabatic heating is computed from the GCM simulations described in the main text. The zonal-mean winds and temperature are nudged toward the GCM-simulated boreal winter ones with a time scale of 3 and 15 days, respectively, following the approaches described in Held and Suarez (1994). For each experiment, the model is integrated for 2000 days, and the last 1000 days are analyzed.

This idealized model differs from the nonlinear stationary wave model used in Held et al. (2002) in a few key aspects. It does not explicitly consider topography, which, though known to be a source of stationary Rossby waves, is not the focus of the current study. As the damping of transients is much weaker than in Held et al. (2002), baroclinic eddies are of comparable strength to those in the full GCM simulations, and act to affect the stationary wave pattern (e.g., Hoerling and Ting 1994). The presence of transient eddies also makes it necessary to average over a longer time period. The zonally

asymmetrical diabatic heating controls regional baroclinicity and thus the locations of storm tracks (e.g., Hoskins and Valdes 1990).

REFERENCES

Alexander, M. A., I. Blade, M. Newman, J. R. Lanzante, N. C. Lau, and J. D. Scott, 2002: The atmospheric bridge: The influence of ENSO teleconnections on air–sea interaction over the global oceans. *J. Climate,* **15,** 2205–2231.

Chen, G., and I. M. Held, 2007: Phase speed spectra and the recent poleward shift of Southern Hemisphere surface westerlies. *Geophys. Res. Lett.,* **34,** L21805, doi:10.1029/2007GL031200.

——, J. Lu, and D. M. W. Frierson, 2008: Phase speed spectra and the latitude of surface westerlies: Interannual variability and global warming trend. *J. Climate,* **21,** 5942–5959.

Feichter, J., E. Roeckner, U. Lohmann, and B. Liepert, 2004: Nonlinear aspects of the climate response to greenhouse gas and aerosol forcing. *J. Climate,* **17,** 2384–2398.

Fischer-Bruns, I., D. F. Banse, and J. Feichter, 2009: Future impact of anthropogenic sulfate aerosol on North Atlantic climate. *Climate Dyn.,* **32,** 511–524.

Forster, P., and Coauthors, 2007: Changes in atmospheric constituents and in radiative forcing. *Climate Change 2007: The Physical Science Basis,* S. Solomon et al., Eds., Cambridge University Press, 129–234.

Frierson, D. M. W., J. Lu, and G. Chen, 2007: Width of the Hadley cell in simple and comprehensive general circulation models. *Geophys. Res. Lett.,* **34,** L18804, doi:10.1029/2007GL031115.

Fu, Q., C. M. Johanson, J. M. Wallace, and T. Reichler, 2006: Enhanced mid-latitude tropospheric warming in satellite measurements. *Science,* **312,** 1179.

GFDL Global Atmospheric Model Development Team, 2004: The new GFDL global atmosphere and land model AM2-LM2: Evaluation with prescribed SST simulations. *J. Climate,* **17,** 4641–4673.

Hall, N. M. J., B. J. Hoskins, P. J. Valdes, and C. A. Senior, 1994: Storm tracks in a high-resolution GCM with doubled carbon dioxide. *Quart. J. Roy. Meteor. Soc.,* **120,** 1209–1230.

Hansen, J., and Coauthors, 2005: Efficacy of climate forcings. *J. Geophys. Res.,* **110,** D18104, doi:10.1029/2005JD005776.

Haywood, J. M., V. Ramaswamy, and B. J. Soden, 1999: Tropospheric aerosol climate forcing in clear-sky satellite observations over the oceans. *Science,* **283,** 1299–1303.

——, L. J. Donner, A. Jones, and J.-C. Golaz, 2009: Global indirect radiative forcing caused by aerosols: IPCC (2007) and beyond. *Clouds in the Perturbed Climate System,* J. Heintzenberg and R. Charlson, Eds., MIT Press, 451–468.

Held, I. M., and M. J. Suarez, 1994: A proposal for the intercomparison of the dynamical cores of atmospheric general circulation models. *Bull. Amer. Meteor. Soc.,* **75,** 1825–1830.

——, and B. J. Soden, 2006: Robust responses of the hydrological cycle to global warming. *J. Climate,* **19,** 5686–5699.

——, M. Ting, and H. Wang, 2002: Northern winter stationary waves: Theory and modeling. *J. Climate,* **15,** 2125–2144.

Hoerling, M. P., and M. Ting, 1994: Organization of extratropical transients during El Niño. *J. Climate,* **7,** 745–766.

Horowitz, L. W., 2006: Past, present, and future concentrations of tropospheric ozone and aerosols: Methodology, ozone evaluation, and sensitivity to aerosol wet removal. *J. Geophys. Res.,* **111,** D22211, doi:10.1029/2005JD006937.

Hoskins, B. J., and P. J. Valdes, 1990: On the existence of storm tracks. *J. Atmos. Sci.,* **47,** 1854–1864.

Hu, Y. Y., and Q. Fu, 2007: Observed poleward expansion of the Hadley circulation since 1979. *Atmos. Chem. Phys.,* **7,** 5229–5236.

James, I. N., 1987: Suppression of baroclinic instability in horizontally sheared flows. *J. Atmos. Sci.,* **44,** 3710–3720.

Johanson, C. M., and Q. Fu, 2009: Hadley cell widening: Model simulations versus observations. *J. Climate,* **22,** 2713–2725.

Krisjánsson, J. E., T. Iversen, A. Kirkevåg, O. Seland, and J. Debernard, 2005: Response of the climate system to aerosol direct and indirect forcing: Role of cloud feedbacks. *J. Geophys. Res.,* **110,** D24206, doi:10.1029/2005JD006299.

Kushner, P. J., I. M. Held, and T. L. Delworth, 2001: Southern Hemisphere atmospheric circulation response to global warming. *J. Climate,* **14,** 2238–2249.

Lau, N. C., 1997: Interactions between global SST anomalies and the midlatitude atmospheric circulation. *Bull. Amer. Meteor. Soc.,* **78,** 21–33.

Lindzen, R. S., and B. Farrell, 1980: A simple approximate result for the maximum growth rate of baroclinic instabilities. *J. Atmos. Sci.,* **37,** 1648–1654.

Lorenz, D. J., and E. T. DeWeaver, 2007: The tropopause height and the zonal wind response to global warming in the IPCC scenario integrations. *J. Geophys. Res.,* **112,** D10119, doi:10.1029/2006JD008087.

Lu, J., G. A. Vecchi, and T. Reichler, 2007: Expansion of the Hadley cell under global warming. *Geophys. Res. Lett.,* **34,** L06805, doi:10.1029/2006GL028443.

——, G. Chen, and D. M. Frierson, 2008: Response of the zonal mean atmospheric circulation to El Niño versus global warming. *J. Climate,* **21,** 5835–5851.

Manabe, S., and R. T. Wetherald, 1975: The effect of doubling CO_2 concentration on the climate of the general circulation model. *J. Atmos. Sci.,* **32,** 3–15.

Ming, Y., and V. Ramaswamy, 2009: Nonlinear climate and hydrological responses to aerosol effects. *J. Climate,* **22,** 1329–1339.

——, and ——, 2011: A model investigation of aerosol-induced changes in tropical circulation. *J. Climate,* **24,** 5125–5133.

——, ——, L. J. Donner, and V. T. J. Phillips, 2006: A new parameterization of cloud droplet activation applicable to general circulation models. *J. Atmos. Sci.,* **63,** 1348–1356.

——, ——, ——, ——, S. A. Klein, P. A. Ginoux, and L. W. Horowitz, 2007: Modeling the interactions between aerosols and liquid water clouds with a self-consistent cloud scheme in a general circulation model. *J. Atmos. Sci.,* **64,** 1189–1209.

Phillips, N. A., 1954: Energy transformations and meridional circulations associated with simple baroclinic waves in a two-level quasi-geostrophic model. *Tellus,* **6,** 273–286.

Reichler, T., M. Dameris, and R. Sausen, 2003: Determining the tropopause height from gridded data. *Geophys. Res. Lett.,* **30,** 2042, doi:10.1029/2003GL018240.

Rotstayn, L. D., and U. Lohmann, 2002: Tropical rainfall trends and the indirect aerosol effect. *J. Climate,* **15,** 2103–2116.

Simmons, A. J., and D. M. Burridge, 1981: An energy and angular-momentum conserving vertical finite-difference scheme and hybrid vertical coordinates. *Mon. Wea. Rev.,* **109,** 758–766.

Toggweiler, J. R., J. L. Russell, and S. R. Carson, 2006: Midlatitude westerlies, atmospheric CO_2, and climate change during the ice ages. *Paleoceanography,* **21,** PA2005, doi:10.1029/2005PA001154.

Vecchi, G. A., A. Clement, and B. J. Soden, 2008: Examining the tropical Pacific's response to global warming. *Eos, Trans. Amer. Geophys. Union,* **89,** 81–83.

Williams, G. P., and K. Bryan, 2006: Ice age winds: An aquaplanet model. *J. Climate,* **19,** 1706–1715.

Williams, K. D., A. Jones, D. L. Roberts, C. A. Senior, and M. J. Woodage, 2001: The response of the climate system to the indirect effects of anthropogenic sulfate aerosol. *Climate Dyn.,* **17,** 845–856.

World Meteorological Organization, 1957: Meteorology—A three-dimensional science: Second session of the commission for aerology. *WMO Bull.,* **4,** 134–138.

Yin, J. H., 2005: A consistent poleward shift of the storm tracks in simulations of 21st century climate. *Geophys. Res. Lett.,* **32,** L18701, doi:10.1029/2005GL023684.